Decision Fusion of Micro-Variability and Signal Averaged ECG Parameters from the QRS Complex with RBF Networks

HA Kestler[1,2], A Müller[1], V Hombach[2], J Wöhrle[2], O Grebe[2], G Palm[1], M Höher[2], F Schwenker[1]

[1]Neural Information Processing, University of Ulm, Germany
[2]Medicine II – Cardiology, University Hospital Ulm, Germany

Abstract

Two types of measurements are usually performed from high resolution ECG recordings: (a) static parameters derived from the signal-averaged QRS complex and (b) variant markers derived from beat-to-beat recordings. It is known that an increased QRS micro-variability and ventricular late potentials are associated with an increased risk for malignant arrhythmias. However, the diagnostic power of the singular parameters is limited. In this study we investigated the diagnostic ability of a decision fusion of both variant and static high-resolution ECG parameters with radial-basis-function (RBF) networks. Continuous and signal-averaged ECGs were recorded from 51 healthy volunteers without any structural heart disease and no cardiac risk factors and from 44 patients with coronary heart disease and ventricular arrhythmias. Beat-to-beat micro-variability measurement of the QRS complex and the ST-T segment was based on 250 consecutive sinus beats per individual. Signal-averaged ECGs were analyzed with the Simson method (QRSD, RMS, LAS). Two RBF networks were trained. One on the three signal averaged parameters and one with the 141D variability vector. The two soft decisions from each RBF network were then combined by average fusion and maximum detection into a final crisp decision which resulted in an unusually high discriminative accuracy.

1. Background

High-resolution electrocardiography is used for the detection of fractionated micropotentials, which serve as a non-invasive marker for an arrhythmogenic substrate and for an increased risk for malignant ventricular tachyarrhythmias. Beat–to–beat variation of cardiac excitation and depolarization has been associated with electrical instability and an increased risk for arrhythmias [1]. Rosenbaum et al. [2] have shown that increased beat–to–beat microvariations of the T–wave, although visually inapparent, are associated with a decreased arrhythmia–free survival. Their method to quantify periodic electrical alternans of the T–wave amplitude has gained growing clinical acceptance as a non–invasive, electrocardiographic risk marker. Earlier high–resolution electrocardiographic studies already demonstrated periodic and non-periodic behaviour of ventricular late potentials at the terminal QRS [3–6]. Previous work of our group showed a significantly higher beat–to–beat variation of the duration of the filtered QRS [7] and an increased total beat–to–beat microvolt variation of the QRS [8] among patients with an increased risk for ventricular tachycardias.

The aim of this study was to utilize and evaluate the combination of static (signal-averaged) and dynamic (beat-to-beat) markers solely based on the QRS complex for subject discrimination.

2. Subject data

We compared a group of 51 healthy subjects (group A) with 44 cardiac patients at a high risk for malignant ventricular arrhythmias (group B, VT patients). All healthy volunteers (mean age 24.0 ± 4.1years) had a normal resting ECG and a normal echocardiogram, and no cardiac symptoms or coronary risk factors. The patients with a high–risk for malignant ventricular arrhythmias (mean age 61.2 ± 8.9 years) were selected from our electrophysiologic database. Inclusion criteria were the presence of coronary artery disease, a previous myocardial infarction, a history of at least one symptomatic arrhythmia, and inducible sustained ventricular tachycardia (> 30 seconds) at electrophysiologic testing. Patients with bundle branch block or atrial fibrillation were excluded. All patients of group B underwent coronary angiography and programmed right ventricular stimulation due to clinical indications. Stimulation was done from the right apex and the right outflow tract. The stimulation protocol included up to 3 extrastimuli during sinus rhythm and at baseline pacing with a cycle length of 500ms, and a maximum of 2 extrastimuli at baseline pacing with cycle lengths of 430ms, 370ms, and 330ms. Group B consisted of 10 patients with single vessel disease, 17 patients with double vessel disease, and 17 patients with triple

0276–6547/02 $17.00 © 2002 IEEE

Computers in Cardiology 2002;29:297–300.

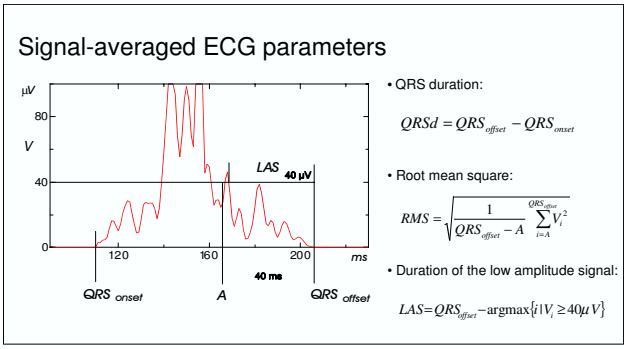

Figure 1. Parameters from the signal-averaged high-resolution ECG: Duration of the QRS complex (QRSd), and amplitude (RMS) and duration (LAS) of the terminal portion of the QRS which are used for ventricular late potential analysis.

vessel coronary artery disease. Nineteen patients had a previous posterior infarction, 14 patients had a previous anterior infarction, and 11 patients had both a previous anterior and a previous posterior infarction. Mean left ventricular ejection fraction was 44.0%±14.9%. Forty-one patients had a documented episode of spontaneous, sustained ventricular tachycardia or ventricular fibrillation. Out of the remaining three patients, 1 patient had syncopes and non–sustained ventricular tachycardias on Holter monitoring, and 2 patients had syncopes of presumed cardiac origin.

3. ECG recordings

High–resolution electrocardiograms were recorded during sinus rhythm from bipolar orthogonal X, Y, Z leads using the Predictor system (Corasonix Inc., Oklahoma, USA). A/D resolution was 16 bit with an antialiasing filter (0.05-300Hz). Before ECG recording antiarrhythmic drugs were stopped for at least four half–lives. The skin was carefully prepared and recordings were done with the subjects in reclining position in a Faraday cage. For signal-averaged recordings the sampling rate was 2000Hz. The three leads were combined into a vectormangnitude signal $V = \sqrt{X^2 + Y^2 + Z^2}$ and bidirectionally filtered with a 4 pole Butterworth filter (40-250Hz), see Figure 1. From this signal the three features of ventricular late potential analysis, QRS duration (QRSd), and the duration (LAS) and amplitude (RMS) of the terminal portion of the QRS complex were extracted. For the beat–to–beat recordings of 30min duration the sampling rate was reduced to 1000Hz. QRS triggering, reviewing of the ECG, and arrhythmia detection was done on a high–resolution ECG analysis platform developed by our group [9]. The three leads were summed into a signal $V = X + Y + Z$. From each recording 250 consecutive sinus beats preceded by another sinus beat were selected

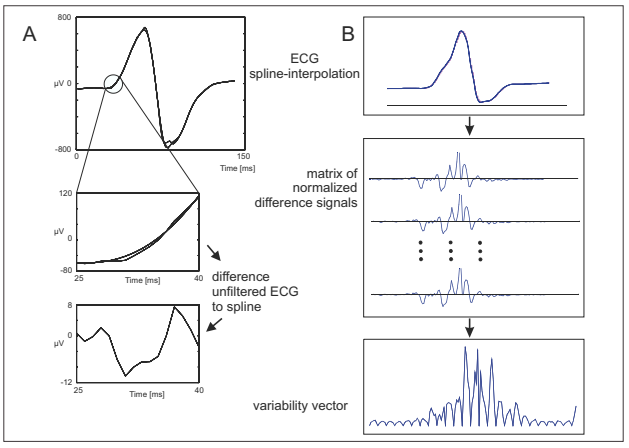

Figure 2. Diagram of the spline–filtering procedure. The upper left panel (A) shows both signals, the QRS–complex (sum of the three leads) and the cubic spline. A zoom–in makes the differences more apparent. The right panel (B) shows the calculation of the variability vector.

for subsequent beat–to–beat variability analysis. In a first step the signals were aligned by maximizing the cross–correlation function [10] between the first and all following beats. Prior to the quantification of signal variability the beats were pre-processed to suppress the main ECG waveform, bringing the beat–to–beat micro-variations into clearer focus. To achieve this, the individual signal was subtracted from its cubic spline smoothed version (spline filtering, spline interpolation through every seventh sample using the not–a–knot end condition) [11], compare Figure 2 panel (A). This method resembles a waveform adaptive, high–pass filtering without inducing phase–shift related artefacts. Next, for each individual beat the amplitude of the difference signal was normalized to zero mean and a standard deviation of 1μV, see Figure 2 panel B. Beat–to–beat variation of each point was measured as the standard deviation of the amplitude of corresponding points across all 250 beats. For the QRS we used a constant analysis window of 141 ms which covered all QRS complexes of this series, thus resulting in a 141 dimensional feature vector [8].

4. RBF classifiers

In the classification scenario a neural network performs a mapping from a continuous input space X $(= \mathbb{R}^d)$ into a finite set of classes $Y = \{\omega_1, \ldots, \omega_l\}$. In the training phase the parameters of the network are determined from a finite training set: $S = \{(\mathbf{x}^\mu, \omega^\mu) | \mu = \mathbf{1}, \ldots \mathbf{N}\}$, each feature vector $\mathbf{x}^\mu \in \mathbb{R}^{\mathbf{d}}$ is labeled with its class membership $\omega^\mu \in Y$. In the recall phase further unlabeled observations $\mathbf{x} \in \mathbb{R}^{\mathbf{d}}$ are presented to the network which estimates their class membership ω. Here, we restrict

ourselves to Gaussian basis functions [12] of the type given in Figure 3. In our classification scenario the number of output units corresponds to the number of classes (1 of l coding). Categorization is performed by assigning the input vector $\mathbf{x}$ the class of the output unit with maximum activation.

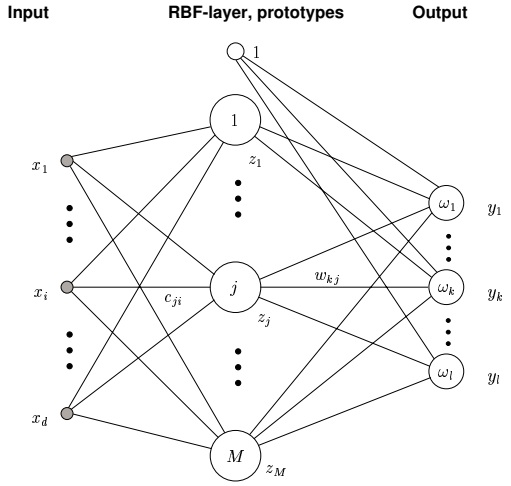

Figure 3. Architecture of the radial basis function neural network with Gaussian basis functions $z_j = \phi_j(\mathbf{x}) = \exp\left(-\frac{||\mathbf{x}-\mathbf{c_j}||^2}{\mathbf{2}\sigma_\mathbf{j}^\mathbf{2}}\right)$ and linear output units $y_k(\mathbf{x}) = \sum_{\mathbf{j=1}}^{\mathbf{M}} \mathbf{w_{kj}}\phi_\mathbf{j}(\mathbf{x}) + \mathbf{w_{k0}}$, $||.||$ denotes the Euclidean norm.

5. Fusion methods

There are different fusion methods for combining features:

1. **Data fusion** is the combination of a set of different feature vectors, e.g. concatenating feature vectors into a single feature vector.
2. **Decision fusion** is the combination of a set of classifier decisions based on different feature detectors into a single decision.

Basically, two different types of classifier combination can be distinguished [13]:

1. Combination with a fixed combination rule or mapping, for instance averaging or multiplying the classifier outputs.
2. Adaptable combination mappings, for instance decision templates or naive Bayes rule. For this, an additional optimization procedure is necessary. Typically, some kind of confusion matrix is calculated based on an extra dataset.

Given P different extracted features, a set of classes $\{1, \ldots, L\}$, and P probabilistic classifiers $C_1, \ldots, C_P$. The outputs of the P different classifiers (one per feature) are called *decision profile* and are given by

$$DP(x) = \begin{bmatrix} y_1^1 & \ldots & y_j^1 & \ldots & y_L^1 \\ \ldots & \ldots & \ldots & \ldots & \ldots \\ y_1^i & \ldots & y_j^i & \ldots & y_L^i \\ \ldots & \ldots & \ldots & \ldots & \ldots \\ y_1^o & \ldots & y_j^P & \ldots & y_L^P \end{bmatrix} \quad (1)$$

here L the number of classes, and $C^i(x_i) = y^i = (y_1^i, \ldots, y_L^i)$ is the output of the i-th classifier with $y_j^i \in [0, 1]$ all i and j, and $\sum_j y_j^i = 1$ all i.

Combination of the classifier outputs can be achieved through several fusion mappings, e.g. *averaging*, which we apply here. The classifier outputs is then given by

$$\tilde{y}_j(x) = \frac{1}{P}\sum_{i=1}^{P} y_j^i. \quad (2)$$

6. Average fusion of RBF networks

The decision fusion of the 3-dimensional and the 141-dimensional data set was performed as follows: For each dataset an independent RBF network with was constructed (one with 3 input neurons and one with 141 input neurons), both networks had the same number of hidden neurons (prototypes) and output neurons each. The RBF neurons used the function $\phi_j(\mathbf{x})$ and the output neurons were linear with the threshold value.

The networks were trained independent according to the following steps:

1. Set initial prototype locations with a K-nearest neighbor algorithm with $K = 5$: Select a randomly chosen data point from the training set and check if the majority of the 5 nearest neighbors would be classified right according to the class label of the observed data point.
2. Train prototypes (hidden neurons) with OLVQ1 (the initial learning rate was set to 0.3, the number of learning steps was 60 times the number of prototypes following a recommendation of Kohonen).
3. Initialize weights between hidden neurons and output layer with uniformly distributed random values in the interval $(-0.5E-7, 0.5E-7)$.
4. The size of the RBF centers were initialized with a value proportional to the mean Euclidean distance to the 3 nearest prototypes with a lower boundary of $1E-20$.
5. The network was fully trained with
6. Armijo line-search following [14], [15], [16] with parameters $\gamma_0 = 0.2$, a step lower bound of 0.04, a maximum of 24 line-search (armijo) steps and a maximum of 100 overall training iterations.

Now the corresponding outputs (matching the classes) of the two networks were combined via average fusion and final crisp decision was generated through a maximum

Decision fusion beat-to-beat and signal averaged data

	Acc	Sensi	Speci
Re-val	95.6% ± 0.44%	90.5% ± 0.96%	100% ± 0.0%
Cross-val	90.4% ± 1.9%	83.4% ± 2.6%	96.5% ± 2.2%
	PPV	NPV	
Re-val	100% ± 0.0%	92.4% ± 0.69%	
Cross-val	95.4% ± 2.9%	87.1% ± 1.9%	

Table 1. Results of the average RBF fusion of two networks with 14 prototypes. Acc: accuracy, Sensi: sensitivity, Speci: specificity, PPV: positive predictive value, NPV: negative predictive value, Re-val: training and test on the same data, Cross-val: 10-fold cross-validation (mean ± stdv, 10 repetitions)

detection. All re-validation and a 10-fold cross-validation runs were repeated 10 times with varying prototype numbers from 2 to 20 for both networks. Table 1 gives the results above 90% cross-validation accuracy with the least number of prototypes.

Data fusion beat-to-beat and signal averaged data

	Acc	Sensi	Speci
Re-val	89.5%	86.4%	92.2%
Cross-val	87.3%±0.61%	86.3%±0.44%	88.1%±1.09%
	PPV	NPV	
Re-val	90.5%	88.7%	
Cross-val	86.3%±1.08%	88.2%±0.38%	

Table 2. Classification results for the linear model of Kestler et al. [17]. Re-val: training and test on the same data, Cross-val: 10-fold cross-validation (mean ± stdv, 1000 repetitions)

7. Conclusion

Soley based on features extracted from the QRS a remarkable classification accuracy of slightly over 90% was attained in the discrimination of healthy from VT/VF patients. Interestingly, this even tops the performance achieved in a earlier study of data fusion including the beat-to-beat variability index derived from the ST-T segment. This results also indicates that the variability vector of the QRS used in this investigation, containes additional information not utilizeable in the QRS variability index.

References

[1] Smith J, Clancy E, Valeri C, Ruskin J, Cohen R. Electrical alternans and cardiac electrical instability. Circulation 1988;77(1):110–121.

[2] Rosenbaum D, Jackson L, Smith J, Garan H, Ruskin J, Cohen R. Electrical Alternans and Vulnerability to Ventricular Arrhythmias. N Engl J Med 1994;330(4):235–41.

[3] Hombach V, Kebbel U, Höpp HW, Winter U, Hirche H. Noninvasive beat-by-beat registration of ventricular late potentials using high resolution electrocardiography. Int J Cardiol 1984;6:167–183.

[4] Hombach V, Kochs M, Höpp HW, Kebbel U, Eggeling T, Osterspey A, Hirche H, Hilger HH. Dynamic behavior of ventricular late potentials. In Hombach V, Hilger HH, Kennedy HL (eds.), Electrocardiography and cardiac drug therapy. Dordrecht, Netherlands: Kluwer Academic Publishers, 1989; 218–238.

[5] Sherif NE, Gomes J, Restivo M, Mehra R. Late potentials and arrhythmogenesis. Pacing Clin Electrophysiol 1985; 8:440.

[6] Sherif NE, Gough W, Restivo M, Craelius W, Henkin R, Caref E. Electrophysiological basis of ventricular late potentials. Pacing Clin Electrophysiol 1990;13:2140–7.

[7] Höher M, Axmann J, Eggeling T, Kochs M, Weismüller P, Hombach V. Beat-to-beat variability of ventricular late potentials in the unaveraged high resolution electrocardiogram - effects of antiarrhythmic drugs. Eur Heart J 1993;14:E:33–39.

[8] Kestler HA, Wöhrle J, Höher M. Cardiac vulnerability assessment from electrical microvariability of the high-resolution electrocardiogram. Medical Biological Engineering Computing 2000;38:88–92.

[9] Ritscher DE, Ernst E, Kammrath HG, Hombach V, Höher M. High–Resolution ECG Analysis Platform with Enhanced Resolution. Computers in Cardiology 1997; 24:291–294.

[10] van Bemmel J, Musen M (eds.). Handbook of Medical Informatics. Heidelberg / New York: Springer Verlag, 1997.

[11] de Boor C. A Practical Guide to Splines. Springer Verlag, 1978.

[12] Bishop C. Neural Networks for Pattern Recognition. Oxford, UK: Oxford University Press, 1995.

[13] Kuncheva LI. Fuzzy Classifier Design. Heidelberg: Physica-Verlag, 2000.

[14] Armijo L. Minimization of functions having Lipschitz continuous first partial derivatives. Pacific Journal of Mathematics 1966;16(1):1–3.

[15] Stoer J. Numerische Mathematik 1. Berlin: Springer, 1994.

[16] Magoulas G, Vrahatis M, Androulakis G. Effective Backpropagation Training with Variable Stepsize. Neural Networks 1997;10(1):69–82.

[17] Kestler HA, Schwenker F, Wöhrle J, Hombach V, Palm G, Höher M. Combined Assessment of Beat-to-Beat Micro-Variability and Signal-Averaged ECG Parameters. Computers in Cardiology 2001;28:73–76.

Address for correspondence:

Hans A. Kestler
Dept. of Neural Information Processing / University of Ulm
D-89069 Ulm / Germany
tel./fax: ++49 (0)731 50024437 / 5024156
kestler@neuro.informatik.uni-ulm.de
hans.kestler@medizin.uni-ulm.de